IEEE/RSJ International Conference on Intelligent Robots and Systems, IROS 97
Grenoble, France, September, 1997

Dynamic Manipulability Analysis of Compliant Motion

Ralf Koeppe
German Aerospace Research Establishment (DLR)
Institute of Robotics and System Dynamics
82230 Wessling, Germany
Email: Ralf.Koeppe@dlr.de

Tsueno Yoshikawa
Department of Mechanical Engineering
Kyoto University
Kyoto 606, Japan
Email: yoshi@mech.kyoto-u.ac.jp

Abstract

Compliant motion tasks can be programmed by human demonstration without the use of the actual robot system. In space applications and sensor off-line programming systems the task is planned and programmed in a virtual reality environment which simulates the world model of the task to be performed. Furthermore in industrial and service applications teach devices measuring the force and motion of the human hand allow the operator to demonstrate a task in a very natural way. By using dynamic manipulability analysis of motion and force, we investigate if a compliant motion trajectory obtained by above described demonstration processes can be executed on a given robot. We analyze the maximum task workspace of executability, the optimal robot-task configuration and the range of necessary or possible scaling factors for motion and forces. The approach is demonstrated using a numerical example.

1 Introduction

Programming robots to execute compliant motion tasks using sensory feedback loops can be solved by observation of an human expert, recording sensorimotion data representing the experts task and generating control laws for the robot from it automatically. With recent advances in virtual reality technology, haptics and human interface systems, demonstration can be performed by the human without the actual robot system. The major advantage is that the dynamics of the demonstration process can be designed to support the human operator. The task can be demonstrated by the expert in a very natural way without being deteriorated by the dynamics of the execution system. Examples of task demonstrations in such a natural way are the interaction with a virtual environment through some virtual display device [1], or direct teaching using a teach device measuring the force and motion of the human hand [2]. An important problem we encounter by following the natural teaching approaches is whether and under which condition the recorded compliant motion trajectory can be executed on a given robot.

The concept of kinematic manipulability was introduced as an effective means to perform task space analysis of robotic manipulators [3]. Differential kinematics and kineto-static show that the axes of ellipsoids representing the range of applicable velocities and forces coincide, with their magnitude being of inverse proportion [4]. These properties where used to propose task compatibility indices, by viewing the robot as a mechanical transformer from joint to task space [5]. Taking into account manipulator dynamics leads to the derivation of dynamic manipulability ellipsoids [6], representing a measure of the admissible end-effector accelerations along each task space direction for a given set of generalized forces. A related concept is the generalized inertia ellipsoid as a geometric representation for the inertial properties of a manipulator [7]. Another manipulability measure which has been introduced is the acceleration radius, which is defined as the minimum upper bound of the magnitude of end-effector accelerations over the entire manipulator workspace [8]. In the context of planning, optimal motions along specified paths considering actuator limits [9] and the applicability of forces by robots interacting with the environment [10] were studied. The Force-Workspace Approach was proposed to plan tasks of large forces over a large range of motion, without violating actuation limits. Force and actuator constraints are mapped into the systems configuration space to plan paths that avoid these constraint obstacles [11]. Workspace analysis and measures for optimization of redundant manipulator postures for large force applications [12] were performed using kineto-static analysis.

To solve the problem of manipulability of compliant motion trajectories the admissible motion and forces of a manipulator have to be both considered. In section two we use the dynamic manipulability ellipsoid and the force ellipsoid to analyze the maximum applicable accelerations and forces in the orthogonal direction of motion and force of the compliant motion

task and derive manipulability measures. In section three we use these measures to state conditions for task executability, for the maximum task space, for the optimal robot-task configuration and the range of necessary or possible scaling factors for acceleration and forces. Section four illustrates the approach using a numerical example.

2 Manipulability of Compliant Motion

Consider a n DOF manipulator with the joint vector $\boldsymbol{q} \in \boldsymbol{R}^n$ in the n-dimensional joint space. The m dimensional task vector is defined by $\boldsymbol{r} \in \boldsymbol{R}^m (m \leq n)$ and represents the end-effector position and orientation. The kinematic relation between $\boldsymbol{q}$ and $\boldsymbol{r}$ is given by the nonlinear function

$$\boldsymbol{r} = \boldsymbol{F_r}(\boldsymbol{q}). \tag{1}$$

By taking the first and second order derivatives of equation (1) w.r.t. time we obtain

$$\dot{\boldsymbol{r}} = \boldsymbol{J}(\boldsymbol{q})\dot{\boldsymbol{q}}, \tag{2}$$

$$\ddot{\boldsymbol{r}} = \boldsymbol{J}(\boldsymbol{q})\ddot{\boldsymbol{q}} + \dot{\boldsymbol{J}}(\boldsymbol{q})\dot{\boldsymbol{q}}, \tag{3}$$

with $\dot{\boldsymbol{r}}$ and $\ddot{\boldsymbol{r}}$ the end-effector velocity and acceleration, $\dot{\boldsymbol{q}} = d\boldsymbol{q}/dt$ the joint velocity vector and $\boldsymbol{J}(\boldsymbol{q}) \in \boldsymbol{R}^{m \times n}$ the Jacobian matrix.

The dynamic equation of a manipulator with some force vector $\boldsymbol{f}$ acting at the tip of the manipulator is

$$\boldsymbol{\tau} - \boldsymbol{J^T}(\boldsymbol{q})\boldsymbol{f} = \boldsymbol{M}(\boldsymbol{q})\ddot{\boldsymbol{q}} + \boldsymbol{h}(\boldsymbol{q}, \dot{\boldsymbol{q}}) + \boldsymbol{g}(\boldsymbol{q}), \tag{4}$$

with $\boldsymbol{\tau} \in \boldsymbol{R}^n$ the joint driving force vector, $\boldsymbol{M}(\boldsymbol{q}) \in \boldsymbol{R}^{n \times n}$ the inertia matrix, $\boldsymbol{h}(\boldsymbol{q}, \dot{\boldsymbol{q}}) \in \boldsymbol{R}^n$ the vector representing the centrifugal and Coriolis forces and $\boldsymbol{g}(\boldsymbol{q}) \in \boldsymbol{R}^n$ the vector of the gravity forces.

To simplify the presentation of our work the velocity dependent terms in equations (3) and (4) are neglected in the sequel.

2.1 Dynamic-Manipulability Ellipsoid

To derive the dynamic-manipulability ellipsoid (DME) we use equations (3) and (4) and write

$$\ddot{\boldsymbol{r}} = \boldsymbol{J}\boldsymbol{M}^{-1}\tilde{\boldsymbol{\tau}}^{DME}, \tag{5}$$

$$\tilde{\boldsymbol{\tau}}^{DME} = \boldsymbol{\tau} - \boldsymbol{J}^T\boldsymbol{f} - \boldsymbol{g}. \tag{6}$$

By introducing the normalized joint driving forces

$$\hat{\tau}_i = \tilde{\tau}_i^{DME} / \tilde{\tau}_{i,max}^{DME} \tag{7}$$

which satisfy $\|\hat{\boldsymbol{\tau}}\| \leq 1$, where[1] $\|\hat{\boldsymbol{\tau}}\| = (\hat{\boldsymbol{\tau}}^T\hat{\boldsymbol{\tau}})^{1/2}$ and

$$\tilde{\tau}_{i,max}^{DME} = \tau_{i,max} - |\tau_i^*| \tag{8}$$

$$\boldsymbol{\tau}^* = \boldsymbol{J}^T\boldsymbol{f} + \boldsymbol{g} \tag{9}$$

[1]We assume throughout the paper that the coordinate systems have been selected and their units have been normalized in such a way that we can use the norms of the form $\boldsymbol{x}^T\boldsymbol{x}$ for any vector $\boldsymbol{x}$. We also assume that we do not change the coordinate frames and their units from the initial ones.

with $\tau_{i,max}$ the maximum joint driving force of the i-th joint, we can rewrite equation (5)

$$\ddot{\boldsymbol{r}} = \boldsymbol{J}\hat{\boldsymbol{M}}^{-1}\hat{\boldsymbol{\tau}} = \boldsymbol{G}\hat{\boldsymbol{\tau}}, \tag{10}$$

and

$$\hat{\boldsymbol{M}} = \boldsymbol{T_\tau^{DME}}\boldsymbol{M}, \tag{11}$$

$$\boldsymbol{T}_\tau^{DME} = \mathrm{diag}\left(\frac{1}{\tilde{\tau}_{i,max}^{DME}}\right). \tag{12}$$

The set of all end-effector accelerations $\ddot{\boldsymbol{r}}$ that the joint driving force can achieve such that $\|\hat{\boldsymbol{\tau}}\| \leq 1$ is the dynamic-manipulability ellipsoid (DME) described by

$$\ddot{\boldsymbol{r}}^T(\boldsymbol{G})^T(\boldsymbol{G})\ddot{\boldsymbol{r}} \leq 1. \tag{13}$$

The principal axes of the DME are obtained by singular value decomposition of $\boldsymbol{G}$ ([6]).

2.2 Manipulating-Force Ellipsoid

To derive the manipulating-force ellipsoid (MFE) we use equation (3) and (4) and write

$$\boldsymbol{f} = (\boldsymbol{J^T})^{-1}\tilde{\boldsymbol{\tau}}^{MFE}, \tag{14}$$

$$\tilde{\boldsymbol{\tau}}^{MFE} = \boldsymbol{\tau} - \boldsymbol{M}\boldsymbol{J}^{-1}\ddot{\boldsymbol{r}} - \boldsymbol{g}. \tag{15}$$

Analog to the derivation of the DME we introduce the normalized joint driving forces

$$\hat{\tau}_i = \tilde{\tau}_i^{MFE} / \tilde{\tau}_{i,max}^{MFE} \tag{16}$$

and further

$$\tilde{\tau}_{i,max}^{MFE} = \tau_{i,max} - |\tau_i^{**}| \tag{17}$$

$$\boldsymbol{\tau}^{**} = \boldsymbol{M}\boldsymbol{J}^{-1}\ddot{\boldsymbol{r}} + \boldsymbol{g}. \tag{18}$$

We can rewrite equation (14)

$$\boldsymbol{f} = (\hat{\boldsymbol{J}}^T)^{-1}\hat{\boldsymbol{\tau}} = \boldsymbol{H}\hat{\boldsymbol{\tau}}, \tag{19}$$

and

$$\hat{\boldsymbol{J}}^T = \boldsymbol{T_\tau^{MFE}}\boldsymbol{J}^T \tag{20}$$

$$\boldsymbol{T}_\tau^{MFE} = \mathrm{diag}\left(\frac{1}{\tilde{\tau}_{i,max}^{MFE}}\right). \tag{21}$$

The set of all end-effector forces $\boldsymbol{f}$ that the joint driving force can achieve such that $\|\hat{\boldsymbol{\tau}}\| \leq 1$ is the manipulating-force ellipsoid (MFE) described by

$$\boldsymbol{f}^T(\boldsymbol{H})^T(\boldsymbol{H})\boldsymbol{f} \leq 1. \tag{22}$$

The principal axes of the MFE are obtained by singular value decomposition of $\boldsymbol{H}$.

The DME and MFE (Figure 1) do not share the directions of their principal axes nor their magnitude

are of inverse proportion as it is the case in the kinematic and kineto-static analysis. Size and direction of the DME and MFE principal axes are coupled through $\tilde{\boldsymbol{\tau}}^{DME}$ and $\tilde{\boldsymbol{\tau}}^{MFE}$ equations (6) and (15) respectively. E.g. if some time varying force is applied to the manipulator tip the DME will change its size accordingly.

In [13] it was shown that the effect of gravity can be taken into account by translation of the ellipsoid center without affecting its volume. The gravity terms as used in equations (9) and (18) lead to a compression of the ellipsoids. In this sense we consider a more conservative approach.

With the DME and MFE we have an intuitive visualization of the robots capability of performing accelerations and forces in certain directions. If the acceleration and force vector determining the compliant motion task stay within their ellipsoids the task will be executable by the robot. We now proceed to define quantitative measures for compliant motion analysis.

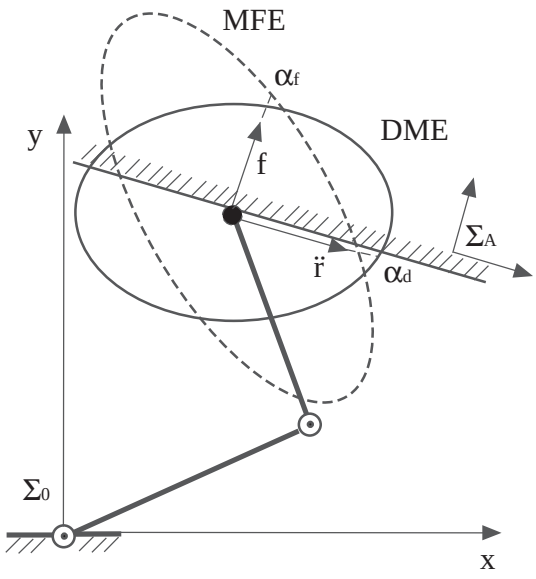

Figure 1: Dynamic-manipulability and manipulating-force ellipsoids in a complaint motion task.

2.3 Admissible Acceleration and Forces

The admissible acceleration radius α_d for a direction represented by the unit vector $\boldsymbol{u}_p$ can be computed from the distance of the origin to the surface of the ellipsoid along $\boldsymbol{u}_p$. Since $\alpha_d \boldsymbol{u}_p$ is a point on the DME it must satisfy according to equation (13)

$$(\alpha_d \boldsymbol{u_p})^T (\boldsymbol{G})^T (\boldsymbol{G})(\alpha_d \boldsymbol{u_p}) = 1. \tag{23}$$

Solving for α_d we get

$$\alpha_d = [\boldsymbol{u_p}^T (\boldsymbol{G})^T (\boldsymbol{G}) \boldsymbol{u_p}]^{-\frac{1}{2}}. \tag{24}$$

Similarly we get for the admissible force radius α_f for direction $\boldsymbol{u_f}$ according to equation (22)

$$(\alpha_f \boldsymbol{u_f})^T (\boldsymbol{H})^T (\boldsymbol{H})(\alpha_f \boldsymbol{u_f}) = 1, \tag{25}$$

and further

$$\alpha_f = [\boldsymbol{u_f}^T (\boldsymbol{H})^T (\boldsymbol{H}) \boldsymbol{u_f}]^{-\frac{1}{2}}. \tag{26}$$

The force radius α_f is essentially the same as the force transmission in [5].

2.4 Acceleration and Force Ratio

We now define the acceleration ratio

$$\kappa_d(t) = \frac{\alpha_d(t)}{\|\ddot{\boldsymbol{r}}(t)\|}, \tag{27}$$

where α_d is computed with $\boldsymbol{u}_p = \ddot{\boldsymbol{r}}/\|\ddot{\boldsymbol{r}}\|$ using equation (24). Similarly we define the force ratio

$$\kappa_f(t) = \frac{\alpha_f(t)}{\|\boldsymbol{f}(t)\|} \tag{28}$$

where α_d is computed with $\boldsymbol{u}_f = \boldsymbol{f}/\|\boldsymbol{f}\|$ using equation (26).

If the vector of interest stays within the ellipsoid limits, $\kappa_i > 1$, where $i = d$ or f. The rest margin, i.e. the distance of the actual vector to the surface of the ellipsoid is $\kappa_i - 1$. If the vector under consideration leaves the ellipsoid boundary, κ_i is in the range $0 < \kappa_i < 1$. Therefore κ_i also gives the scaling factor for the vector to the intersection point of the respective ellipsoid. In this sense finding an optimal configuration results in maximizing the ratio κ_i as described in section 3.4.

2.5 Task Surfaces, Constraints and Uncertainty Measures

So far we have formulated the problem for arbitrary directions of acceleration and force. In a compliant motion task with rigid objects, directions of motion and forces are determined by the task geometry. We consider a compliant motion task that requires $k(\leq 6)$ degrees of freedom. When the manipulator is constrained by a set of $m(\leq k)$ hyper surfaces

$$p_i(\boldsymbol{r}) = 0, \quad i = 1, 2, \ldots, m \tag{29}$$

we can define

$$\boldsymbol{E}_F = [\boldsymbol{e}_{(k+1)-m}, \boldsymbol{e}_{(k+2)-m}, \ldots, \boldsymbol{e}_k]^T, \tag{30}$$

$$\boldsymbol{e}_{k-m+i} = \frac{\partial p_i(\boldsymbol{r})}{\partial \boldsymbol{r}}, \quad i = 1, 2, \ldots, m \tag{31}$$

from the set of directions in which the end-effector is constraint. Similarly if we express the end-effector trajectory on the constraint surface as

$$\boldsymbol{y}_P = \boldsymbol{s}(\boldsymbol{r}) = [s_1(\boldsymbol{r}), s_2(\boldsymbol{r}), \ldots, s_{6-m}(\boldsymbol{r})]^T \tag{32}$$

we can define

$$\boldsymbol{E}_P = [\boldsymbol{e}_1, \boldsymbol{e}_2, \ldots, \boldsymbol{e}_{k-m}]^T, \quad (33)$$

$$\boldsymbol{e}_j = \frac{\partial s_j(\boldsymbol{r})}{\partial \boldsymbol{r}}, \quad j = 1, 2, \ldots, k-m \quad (34)$$

from the set of directions that span the sub-space of the end-effector trajectory. The acceleration of the trajectory can be obtained from equation (32) by differentiating twice w.r.t. time:

$$\ddot{\boldsymbol{y}}_P = \boldsymbol{E}_P \ddot{\boldsymbol{r}} + \dot{\boldsymbol{E}}_P \dot{\boldsymbol{r}}. \quad (35)$$

The following derivations can be made for the case where the term $\dot{\boldsymbol{E}}_P \dot{\boldsymbol{r}}$ in above equation is neglectable. Then the directions defined by equation (31) and (34) define the k dimensional space R^k for the compliant motion task.

From the k dimensional DME we compute the $k-m$ dimensional sub-ellipsoid $\overline{\text{DME}}$ in the subspace formed by the directions $\{\boldsymbol{e}_1, \boldsymbol{e}_2, \ldots, \boldsymbol{e}_{k-m}\}$. Similar we compute from the k dimensional MFE the m dimensional sub-ellipsoid $\overline{\text{MFE}}$ in the subspace formed by the directions $\{\boldsymbol{e}_{(k+1)-m}, \boldsymbol{e}_{(k+2)-m}, \ldots, \boldsymbol{e}_k\}$.

To compute $\kappa_i(t)$ from the acceleration or force vector $\boldsymbol{a}(t)$ in the respective domain, we compute the minimal distance between the sub-ellipsoid and a hyper sphere of the same dimension, with the center determined by the end of the of vector $\boldsymbol{a}(t)$ radius $\|\Delta \boldsymbol{a}\|$ and further

$$\kappa_i(t) = \frac{\alpha_i(t)}{\boldsymbol{a}(t)} = \frac{\|\boldsymbol{a}(t)\| + \|\Delta \boldsymbol{a}(t)\| + d_{min}}{\|\boldsymbol{a}\| + \|\Delta \boldsymbol{a}\|}. \quad (36)$$

The hyper sphere represents the domain of uncertainty of direction and magnitude. If the hyper sphere intersects with the ellipsoid, then $\kappa_i(t)$ is in the range of $0 < \kappa_i(t) < 1$ and the task is not executable.

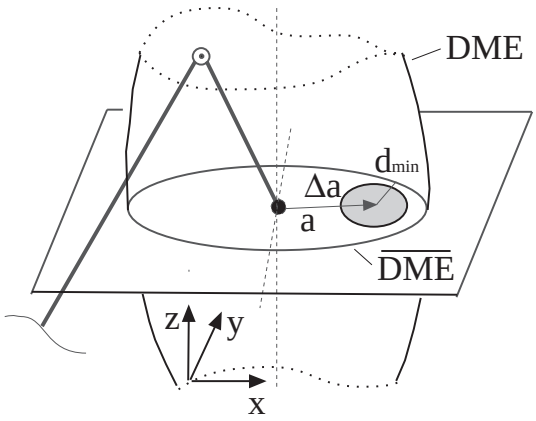

Figure 2: Uncertainty radius and sub-ellipsoids.

Figure 2 gives an example for a compliant motion task with $k = 3$ and $m = 1$. The directions of motion $\boldsymbol{E_P}$ and forces $\boldsymbol{E_F}$ are

$$\boldsymbol{E_P} = \begin{pmatrix} 1 & 0 \\ 0 & 1 \\ 0 & 0 \end{pmatrix}, \qquad \boldsymbol{E_F} = \begin{pmatrix} 0 \\ 0 \\ 1 \end{pmatrix}. \quad (37)$$

The uncertainty region is for the acceleration of $k - m = 2$ dimension. Therefore it is a circle of radius $\|\Delta \boldsymbol{a}(t)\|$ around the acceleration vector $\boldsymbol{a}(t)$.

If the term $\dot{\boldsymbol{E}}_P \dot{\boldsymbol{r}}$ in equation (35) is not neglectable, e.g. in the case of following a curved surface with small radius, the uncertainty analysis for the acceleration space has to be carried out in the DME instead of the sub-ellipsoid $\overline{\text{DME}}$ since the directions specified by $\dot{\boldsymbol{E}}_P$ have to be considered in addition. Hence the dimension of the uncertainty hyper sphere and the DME are the same. The analysis of forces in the domain of the sub-ellipsoid $\overline{\text{MFE}}$ is still valid.

3 Compliant Motion Analysis

3.1 Parameterization of compliant motion tasks

A compliant motion task is defined by the set

$$\{\Sigma_A, {}^A\ddot{\boldsymbol{y}}(t), {}^A\dot{\boldsymbol{y}}(t), {}^A\boldsymbol{y}(t), {}^A\boldsymbol{f_y}(t)\}, \quad (38)$$

defining a motion and force trajectory in a fixed coordinate frame Σ_A. ${}^A\boldsymbol{y}^{(i)}(t)$ denotes the position trajectory (equation (32)) and its ith derivative and ${}^A\boldsymbol{f_y}(t)$ the corresponding force trajectory in directions given by equation (30).

The coordinate transformation ${}^0\boldsymbol{T_A}(\boldsymbol{\pi})$ is parameterized by a vector $\boldsymbol{\pi}$ and determines the pose of the task w.r.t. the robot coordinate system Σ_0, i.e. how the task is placed in the workspace. The compliant motion trajectory in Σ_0 is obtained from

$$\boldsymbol{y}^{(i)}(t) = {}^0\boldsymbol{T_A}(\boldsymbol{\pi}) {}^A\boldsymbol{y}^{(i)}(t), \quad (39)$$

$$\boldsymbol{f_y}(t) = {}^0\boldsymbol{T_A}(\boldsymbol{\pi}) {}^A\boldsymbol{f_y}(t). \quad (40)$$

Given a certain compliant motion trajectory parameterized by $\boldsymbol{\pi}$, we compute for each time t of the compliant motion trajectory the ratios $\kappa_d(t)$ and $\kappa_f(t)$ to perform the following analysis:

3.2 Executability

A compliant motion task can be executed in the workspace location $\boldsymbol{\pi}$ if the following condition holds:

$$\min_{\kappa_d, \kappa_f} [\kappa_{dmin}, \kappa_{fmin}] > 1. \quad (41)$$

with

$$\kappa_{dmin} = \min_t \kappa_d(t), \quad (42)$$

$$\kappa_{fmin} = \min_t \kappa_f(t). \quad (43)$$

I.e. if both trajectories of $\kappa_d(t)$ and $\kappa_f(t)$ are greater then 1, during the execution the task is executable.

3.3 Maximum Task Space

Next we determine the maximum task space where the compliant motion can be executed.

The task space $\mathbf{\Pi} = \{\boldsymbol{\pi}_i^\star\}$ *in which the compliant motion task is executable is defined by*

$$\kappa_{cm}(\boldsymbol{\pi}_i^\star) \triangleq \min_{\kappa_d, \kappa_f} [\kappa_{dmin}(\boldsymbol{\pi}_i^\star), \kappa_{fmin}(\boldsymbol{\pi}_i^\star)] > 1. \quad (44)$$

The task space $\mathbf{\Pi}$ contains all complaint motion task configurations that are executable.

3.4 Optimal Task Configuration

The optimal task configuration $\boldsymbol{\pi}_{opt}^\star$ *is defined by the condition*

$$\max_{\boldsymbol{\pi}_i^\star \in \mathbf{\Pi}} [\kappa_{cm}(\boldsymbol{\pi}_i^\star)]. \quad (45)$$

The criterion of finding the optimal configuration is defined as a min-max problem. It is optimal in the sense of finding the compliant motion configuration that gives maximum acceleration ratio κ_d and force ratio κ_f during execution of the task.

3.5 Scaling

The values of κ_{dmin} and κ_{fmin} obtained by equations (42) and (43) give the maximum scaling of acceleration and forces respectively. Both vector can not be scaled with the maximum values at the same time since in the derivation of the ratios, we have calculated the maximum radius from the DME and MFE which are coupled through equation (6) and (15) respectively as mentioned before. If the task is not executable at least one of the ratios κ_{dmin} and κ_{fmin} is smaller than 1. If acceleration and forces of the task are scaled by their respective ratio the task becomes executable.

4 Numerical Example

We will show the validity of above derived approach using simulations of a two-link manipulator in a horizontal plane as shown in Figure 1. The parameters of the manipulator are (in SI units): the link length $l1 = 1.0$, $l2 = 1.0$, the distance of the center of gravity on the link $l_{g1} = 0.5$, $l_{g2} = 0.3$, the link mass $m_1 = 20$, $m_2 = 10$, the link inertia $\hat{I}_1 = 20/12$, $\hat{I}_2 = 10/12$, the maximum generalized forces $\tau_{1,max} = 350$, $\tau_{2,max} = 150$ and a load mass of $m_l = 5$.

The task is to follow a straight line trajectory of length l in direction $\boldsymbol{E_p} = [1, 0]^T$ on a surface with normal vector $\boldsymbol{E_f} = [0, 1]^T$. The acceleration and force profiles are given as:

$$a(t) = \begin{cases} a, & 0 \le t \le 0.4 \\ 0, & 0.4 < t \le 0.6 \\ -a, & 0.6 < t \le 1.0 \end{cases}$$

$$f(t) = f, \qquad 0 \le t \le 1.0,$$

where t denotes the time. The task acceleration and force trajectory is then defined by ${}^A\ddot{\boldsymbol{y}}(t) = a(t)\boldsymbol{E_p}$ and ${}^A\boldsymbol{f}(t) = f(t)\boldsymbol{E_F}$ respectively. Since the task is $k = 2$ dimensional with $m = 1$ dimension of force, the uncertainty hyper sphere has to be considered only in one dimension for acceleration and force respectively. In this case uncertainty becomes a scalar value. We considered 10% of the values a and f.

A set of minimal parameters specifying the task location in workspace can be defined to $\boldsymbol{\pi} = \{x_m, y_m\}$, since we consider the case of a horizontal plane. The coordinate transformation ${}^0\boldsymbol{T_A}(\boldsymbol{\pi})$ then simply becomes a translation by the vector $[x_m - l/2, y_m]^T$. The length $l/2$ is considered in x direction since we parameterize w.r.t. the center of the straight line. Numerical computations were carried out in the interval $x_m, y_m = [-2.0, 2.0]$.

Figure 3 shows the kinematic feasible region (light gray). However the compliant motion task ($f = 100N$, $a = 6.25m/s^2$ and $l = 1.5m$) is restricted to the maximum task space $\mathbf{\Pi}$ (dark gray) as result of our analysis. Note that the kinematic feasible region is not circular since we consider the task space and not the workspace.

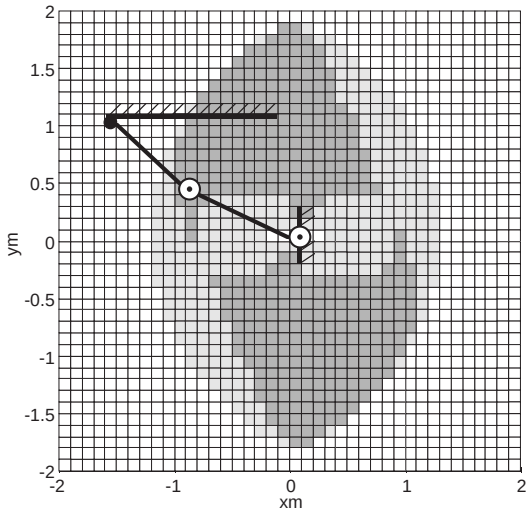

Figure 3: Kinematic feasible region of task (light gray) and Maximum Task Workspace of compliant motion manipulability (dark gray) where the task is executable.

Figure 4 shows for the compliant motion task ($f = 100N$, $a = 6.25m/s^2$ and $l = 1.5m$) (a) the values for $\kappa_{cm}(\boldsymbol{\pi}_i^\star)$, (b) $\kappa_{dmin}(\boldsymbol{\pi}_i^\star)$ and (c) $\kappa_{fmin}(\boldsymbol{\pi}_i^\star)$. Regions of white, gray and black space denote values for $\kappa_i = 0$, $1 < \kappa_i < 2$ and $\kappa_i > 2$ respectively. The figure shows the sensitivity of the compliant motion manipulability measure. It can be seen that around the center of the task space compliant motion manipulability is restricted by the dynamic-manipulability where as the

in the rest of the region the force-manipulating manipulability is clearly the limiting factor.

Figure 5 displays the locus of the optimal task configurations for the compliant motion task with forces of $f = 25, 50, 75, 100N$ ($a = 6.25m/s^2$ and $l = 1.5m$). Table 1 shows that in the case of $f = 75$ and $100N$ κ_{fmin}, and in the case of $f = 25$ and $50N$ κ_{dmin} is the limiting factors.

Finally Figure 6 illustrates the optimal task configuration for (a) $f = 100N$ and (b) $f = 50N$. The solution found by our analysis can be observed in human skills. In applying forces to a straight line edge of a surface, e.g. preparing the steel edge of a ski, human workers straight out their arm to apply higher forces, where as in polishing tasks speed is necessary while maintaining low forces. In this case the human worker positions himself so that his arm motion varies around 90 degrees between the under and the upper part of the arm.

f	xm	ym	κ_{dmin}	κ_{fmin}
100	-0.6	1.4	1.6950	1.4321
75	-0.7	1.2	2.0227	1.8826
50	-0.9	0.9	2.2871	2.3583
25	-1.0	0.1	2.8111	3.9142

Table 1: Optimal configuration $\{x_m, y_m\}$ for different forces f and κ_{dmin}, κ_{fmin} the minimum compliant motion manipulability measures of the compliant motion trajectory.

5 Conclusions

We have proposed a method to investigate the compliant motion manipulability of a given compliant motion trajectory. From the measures we derived analysis of executability, maximum task space, optimal task configuration and scaling properties was carried out. Uncertainty was considered by taking into account the minimal distance between uncertainty hyper spheres of acceleration and force with the dynamic-manipulability sub-ellipsoids and the manipulating-force sub-ellipsoids respectively. The planes of the sub-ellipsoids are determined by the geometry of the compliant motion task. The next step will be the analysis of compliant motion trajectories obtained by human demonstration using a teach device [2].

References

[1] R. Koeppe and G. Hirzinger. Learning compliant motions by task-demonstration in virtual environments. In *Fourth Int. Symp. on Experimental Robotics, ISER, Stanford*, June 30 -July 2 1995.

[2] R. Koeppe, A. Breidenbach, and G. Hirzinger. Skill representation and acquisition of compliant

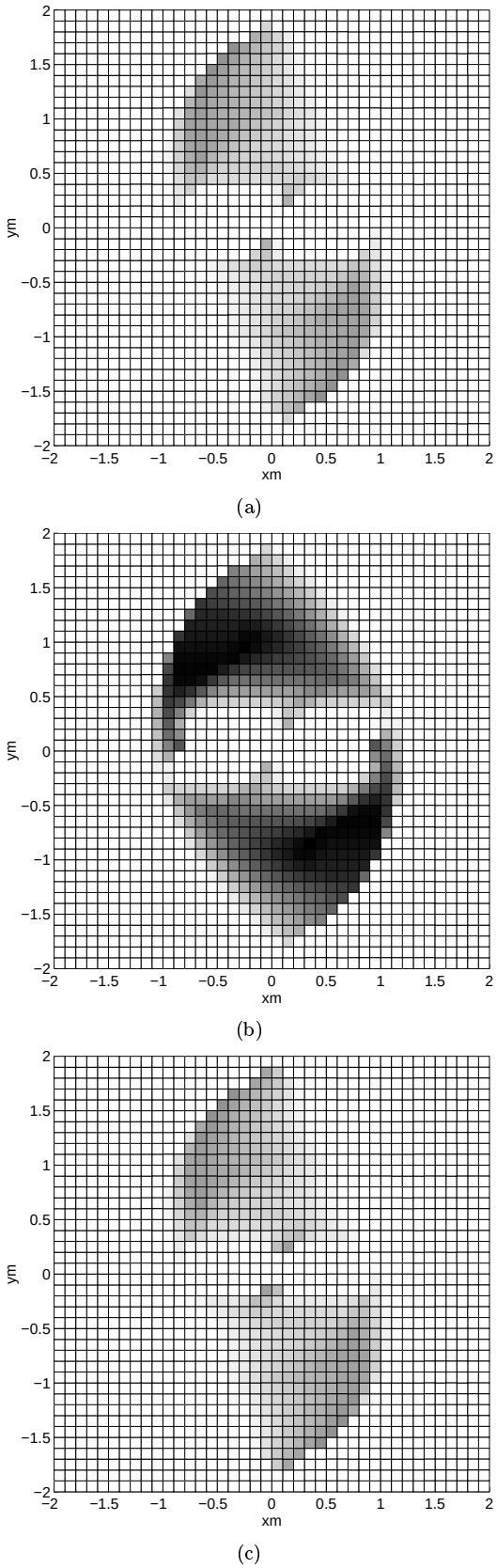

Figure 4: Region Π of compliant motion manipulability: (a) κ_{cm}, (b) $\kappa_{dmin} > 1$, (c) $\kappa_{fmin} > 1$

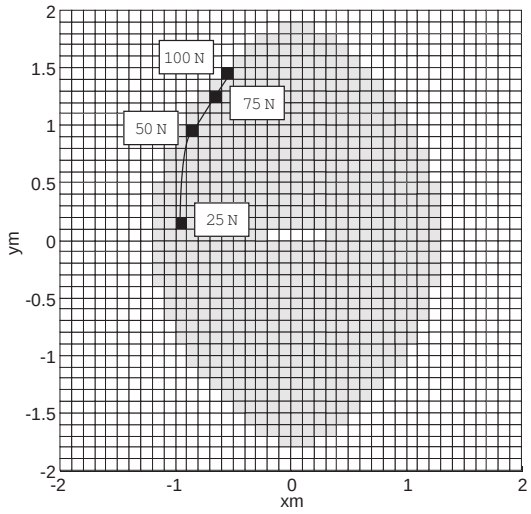

Figure 5: Locus of optimal task configuration for forces $f = 25, 50, 75, 100N$.

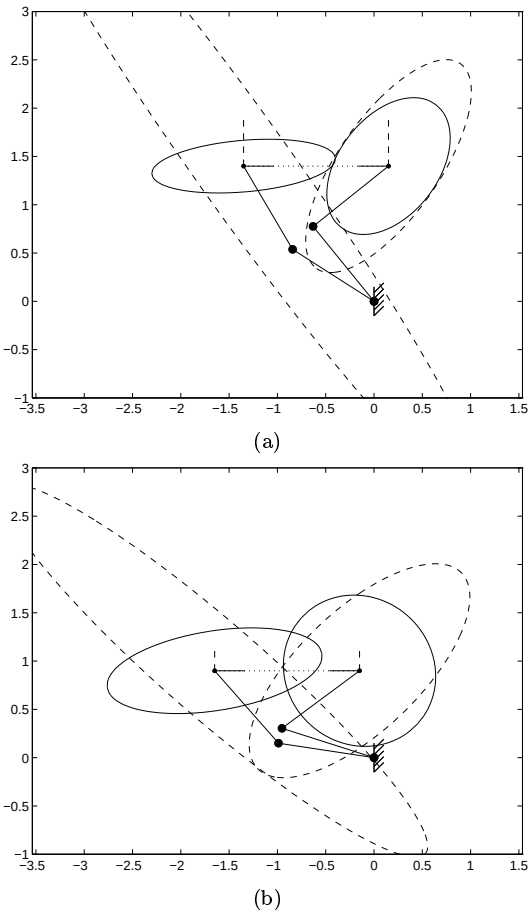

Figure 6: Optimal Task Configuration for case (a) $f =$ 100 N and (b) $f = 50$ N. For each case the start and end configuration and their acceleration, force vectors and ellipsoids are shown (solid: acceleration, dashed: forces).

motions using a teach device. In *IEEE/RSJ Int. Conf. on Intelligent Robots and Systems, IROS, Osaka, Japan*, November 1996.

[3] T. Yoshikawa. Analysis and control of robot manipulators with redundancy. In M. Brady and R. Paul, editors, *Robotics Research: The 1st International Symposium*, pages 735–747. MIT Press, Cambridge, MA, 1984.

[4] T. Yoshikawa. Manipulability of robotic mechanisms. *The International Journal of Robotics Research*, 4:3–9, 1985.

[5] S. L. Chiu. Control of redundant manipulators for task compatibility. In *Proc. of the IEEE Int. Conf. on Robotics and Automation*, pages 1718–1724, 1987.

[6] T. Yoshikawa. Dynamic manipulability of robot manipulators. *Journal of Robotic Systems*, 2:113–124, 1985.

[7] H. Asada. Dynamic hybrid position/force control of robot manipulators-description of hand constraints and calculation of joint driving force. *Transactions of the ASME Journal of Dynamic Systems, Measurement, and Control*, 105, 1983.

[8] T. J. Graettinger and B. H. Krogh. The acceleration radius: A global performance measure for robotic manipulators. *IEEE Journal of Robotics and Automation*, RA-4:60–69, 1988.

[9] J. E. Bobrow and et al. Time-optimal control of robotic manipulators along specified paths. *The International Journal of Robotics Research*, 4, 1985.

[10] Y. Nakamura. Force applicability of robotic mechanisms. In *Proc. 26th Conf. on Decision and Control*, pages 570–575, 1987.

[11] A. Madhani and S. Dubowsky. Motion planning of mobile multi-limb robotic systems subject to force and friction constraints. In *Proc. of the IEEE Int. Conf. on Robotics and Automation*, pages 233–239, 1992.

[12] E. Papadopoulos and Y. Gonthier. On manipulator posture planing for large force tasks. In *Proc. of the IEEE Int. Conf. on Robotics and Automation*, pages 126–131, 1995.

[13] P. Chiacchio, S. Chiaverini, L. Sciavicco, and B. Siciliano. Reformulation of dynamic manipulability ellipsoid for robotic manipulators. In *Proc. of the IEEE Int. Conf. on Robotics and Automation*, pages 2192–2197, 1991.